Effects of Copper on Proeutectoid Cementite Precipitation

J. A. WASYNCZUK, R. M. FISHER, and G. THOMAS

The effect of copper on proeutectoid cementite precipitation was investigated by examining the isothermal transformation characteristics of Fe-C and Fe-C-Cu alloys that had comparable carbon contents. The TTT diagrams generated for the Fe-1.43 wt pct C and the Fe-1.49 wt pct C-4.90 wt pct Cu alloys showed that the kinetics of proeutectoid cementite precipitation were not significantly affected by copper. The morphology of the proeutectoid cementite, as seen in the optical microscope, was also substantially the same in both alloys. However, transmission electron microscopy revealed the presence of small epsilon-copper precipitates within the proeutectoid cementite of the copper containing steel. It was concluded that this precipitation of ε-Cu took place at the cementite:austenite interphase boundaries, and that the transport of copper to the precipitates was accomplished by interphase boundary diffusion. The small influence of copper on the kinetics of proeutectoid cementite precipitation is discussed in terms of diffusional growth theories and the structure of the cementite:austenite interphase boundary.

I. INTRODUCTION

WHEN hypereutectoid steels are cooled from the austenite range, proeutectoid cementite is often precipitated at austenite grain boundaries. The first morphology observed is usually that of grain boundary allotriomorphs.[1] These precipitates nucleate at austenite grain boundaries and grow, more or less smoothly, along them.[2] Lengthening along the grain boundary proceeds more quickly than thickening normal to it, and this causes the allotriomorphs to take the shape of lenses. The allotriomorphs quickly lengthen and impinge upon each other, leaving the grain boundaries covered with thin (on the order of a micron) films of proeutectoid cementite. After longer transformation times, proeutectoid cementite may also precipitate intragranularly, usually in the form of Widmanstätten plates.[1] This evolution of microstructure is analogous to that which occurs during the precipitation of proeutectoid ferrite in hypoeutectoid steels.[2,3] Proeutectoid cementite grain boundary allotriomorphs have been identified as a source of embrittlement in high carbon steels.[4]

Proeutectoid cementite grain boundary allotriomorphs thicken rapidly at first, but much more slowly at the later stages of the transformation.[6] The initial thickening rates have been found to be considerably lower than those calculated under the assumption that growth is controlled exclusively by the diffusion of carbon through austenite.[5,6] Thickening rates lower than those allowed by the diffusion of carbon through austenite have also been found for proeutectoid ferrite grain boundary allotriomorphs in hypoeutectoid steels.[2,3,7] These sluggish thickening kinetics have been attributed to the effects of interphase boundary structure.[2,3,5-7] It is thought that the interphase boundary surrounding grain boundary allotriomorphs consists of a mixture of incoherent and partially coherent portions.[2] The incoherent portions have high mobility and can migrate freely under the action of carbon diffusion.[2] The partially coherent portions are manifested as planar facets which can migrate normal to themselves only by a ledge mechanism.[2,3] The necessity to migrate by a ledge mechanism causes these facets to act as a structural impediment to growth.[2,3] However, the exact amount and distribution of partially coherent facets that exist at the boundary remain uncertain, and this is a central issue concerning the diffusional decomposition of austenite.

Proeutectoid cementite grain boundary allotriomorphs thicken more rapidly in high purity Fe-C alloys than in steels containing approximately 0.23 wt pct Si.[5] Silicon has very little solubility in cementite,[8] and it is thought that the partitioning of silicon away from growing cementite plays a large role in reducing allotriomorph thickening kinetics.[5,9] Conversely, it has been shown that phosphorus can accelerate proeutectoid cementite precipitation.[10] However, the current understanding of the effects of alloy chemistry on proeutectoid cementite precipitation, particularly with regard to how it can be inhibited, is far from complete.

When cementite or ferrite grows into austenite, solutes can be partitioned by the precipitation of third phases at interphase boundaries. The partitioning of silicon at cementite:austenite interphase boundaries can result in the formation of "porous" cementite,[5,11] which is a mixture of cementite and ferrite that has been stabilized by silicon enrichment. Precipitation of alloy carbides,[12,13] epsilon-Cu,[14,15] and gold,[16] *i.e.*, interphase precipitates, at ferrite:austenite interphase boundaries are other examples of solute partitioning by the formation of third phases. One characteristic that appears to be common to all types of interphase precipitates is the adoption of a single variant of a crystallographic orientation relationship with the ferrite.[12-16] The variant chosen is often the one which permits the simultaneous satisfaction of a favorable orientation relationship with the parent austenite.[12,13]

Although the metallography of interphase precipitates has been well documented,[12-16] some uncertainties exist concerning their influence on boundary mobility. It has been suggested that interphase precipitates can effectively pin intrinsically mobile, incoherent boundaries.[17] However,

J. A. WASYNCZUK is with the Department of Materials Science and Mineral Engineering, University of California, Berkeley, CA 94720 and Materials and Molecular Research Division, Lawrence Berkeley Laboratory, 1 Cyclotron Road, Berkeley, CA 94720. R. M. FISHER is Staff Senior Scientist, Center for Advanced Materials, Lawrence Berkeley Laboratory, 1 Cyclotron Road, Berkeley, CA 94720. G. THOMAS is Professor, Department of Materials Science and Mineral Engineering, University of California, Berkeley, CA 94720 and Scientific Director, National Center for Electron Microscopy, Materials and Molecular Research Division, 1 Cyclotron Road, Lawrence Berkeley Laboratory, Berkeley, CA 94720.

Manuscript submitted February 4, 1986.

other results indicate that at least some portions of partially coherent boundary are essential to allow the nucleation of interphase precipitates.[18,19] Since the partially coherent portions of the interphase boundary are inherently immobile in the direction normal to the boundary, precipitation that is confined to them should not represent a structural obstacle to growth. However, interphase precipitates that are confined to the partially coherent portions of the boundary can still alter the rate of boundary migration through their influence on the diffusion gradient of carbon.[20]

The present work was undertaken in order to develop a better understanding of how the partitioning of substitutional solutes influences the kinetics of proeutectoid cementite precipitation. In addition to its significance as a sintering aid in powder metallurgy[21] and as an impurity in recycled steel,[22] copper was chosen as an alloying element because it does not form a stable carbide,[23] and it has very little solubility in cementite.[24] Therefore, there is a strong thermodynamic tendency for it to partition away from cementite. The effect of copper is evaluated by comparing the isothermal transformation kinetics and microstructures of Fe-C and Fe-C-Cu alloys that have similar carbon contents.

Figure 1 shows an 800 °C isothermal section of the Fe-C-Cu phase diagram.[25] Most of the phase boundaries in this diagram were generated from computer calculations in which it was assumed that copper is completely insoluble in cementite. The diagram shows that when both the carbon and copper contents of an alloy are high, the equilibrium state is one in which three phases coexist, austenite, cementite, and ε-Cu. The solubility of carbon in ε-Cu is extremely small, less than one ppm, at 800 °C.[26] The solubility of iron in ε-Cu is also low, less than 1 wt pct, at 800 °C.[26] This phase diagram also indicates that the solubility of carbon in austenite is relatively unaffected by the presence of copper. Because of this, the austenite:(austenite + cementite + ε-Cu) solvus temperature of a hypereutectoid Fe-C-Cu alloy is nearly the same as the austenite:(austenite + cementite) solvus temperature of an Fe-C alloy with identical carbon content. Therefore, the supersaturations of carbon which drive the isothermal precipitation of proeutectoid cementite can be expected to be comparable in Fe-C and Fe-C-Cu alloys that have similar carbon contents.

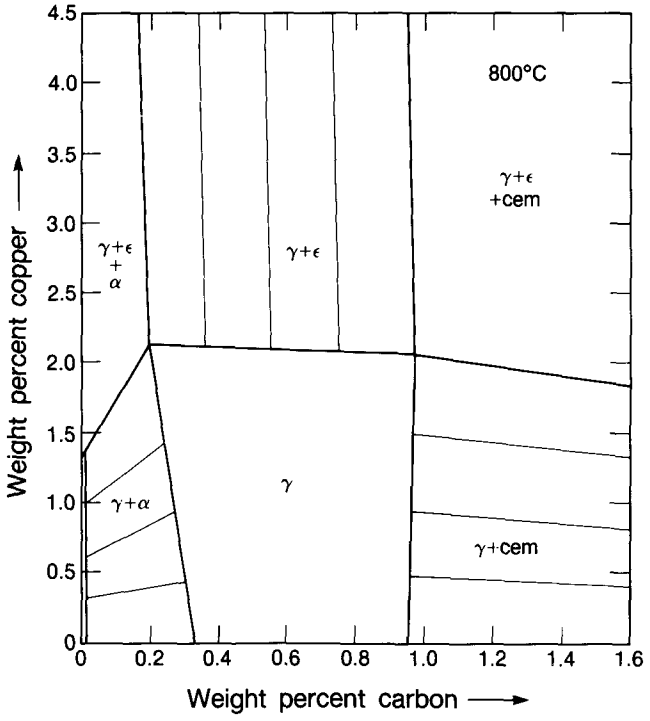

Fig. 1—800 °C isothermal section of the iron-rich portion of the Fe-C-Cu phase diagram. Reproduced from Ref. 25.

II. EXPERIMENTAL PROCEDURE

Three alloys were used in this investigation. Their compositions are listed in Table I. All of the alloys used were of high purity and were vacuum cast. The Fe-1.43C and the Fe-1.31C-3.57Cu alloys were cast as 3 cm diameter, 28 cm long cylindrical ingots. These cylindrical ingots were heated to 1200 °C, under an argon atmosphere, and then hot rolled to 16 mm plate. These 16 mm plates were then homogenized at 1200 °C for 24 hours, under an argon atmosphere, and furnace cooled. The Fe-1.49C-4.90Cu alloy was cast in the form of a 15 mm × 50 mm × 65 mm ingot. It was not hot rolled, but was given the same homogenization treatment as the other alloys.

The isothermal transformation kinetics of the alloys were evaluated by optical metallography. The specimens used were small plates, measuring 0.8 mm × 13 mm × 13 mm. It has been demonstrated that the stereology of grain boundary allotriomorphs is simplified if metallographic specimens are made sufficiently thin to cause the austenite grain boundaries to lie normal to the polished surface.[27] However, because the microstructures being investigated were very brittle, especially with regard to intergranular fracture, it was not practical to prepare large flat areas for optical metallography in specimens thinner than 0.8 mm. For transmission electron microscopy, the specimens started as thin sheets measuring 0.25 mm × 13 mm × 13 mm.

Two techniques were used to perform the isothermal heat treatments. When the duration of the isothermal reaction was less than 30 minutes, the following procedure was used. The heat treatments began with a twenty-minute austenitization at 1150 °C. This was done in a vertical tube furnace under a dynamic argon atmosphere. The temperature was controlled to within ±5 °C. Following austenitization, the specimens were quenched into molten barium chloride salt at temperatures ranging from 600 °C to 850 °C, for times ranging from six seconds to 30 minutes. The temperature was controlled to within ±3 °C. After isothermal reaction in the salt bath, the specimens were quenched into iced-brine. As a precaution against decarburization, a graphite rod was immersed in the molten salt for 24 hours prior to heat treatment.

When the isothermal reactions were longer than 30 minutes, a different procedure was used in order to avoid decarburization. For these heat treatments the specimens were first sealed in evacuated quartz capsules and then austenitized, in a box furnace, at 1150 °C for 30 minutes. The specimens were then quickly transferred to an adjacent box furnace that was maintained at the transformation temperature. The temperature control of the box furnaces was ±3 °C. After isothermal reaction, the specimens were quenched into iced-brine.

Table I. Alloy Compositions (Weight Percent)

Fe	C	Cu	Mn	N	O	P	Si	S
bal.	1.43	<0.005	<0.005	0.003	0.006	<0.005	0.005	<0.002
bal.	1.49	4.90	<0.005	0.001	0.005	<0.005	0.007	0.002
bal.	1.31	3.57	<0.005	0.003	0.003	<0.005	0.005	<0.002

After heat treatment, a broad face of the small plates was prepared for optical metallography by standard grinding and polishing procedures. Nital was used as an etchant. The grinding procedure was sufficient to eliminate all visual signs of decarburization.

The austenitization treatment produced an austenite grain size of approximately 350 microns, which was a little less than half of the specimen thickness. Because the austenite grain boundaries intersected the metallographic plane of polish at a variety of angles, the apparent thickness of the proeutectoid cementite grain boundary allotriomorphs was not the same as their true thickness, normal to the boundary. The true thickness was calculated by the following equation:[5,28]

$$T = \overline{T}/2 \qquad [1]$$

where T = the true thickness of the grain boundary allotriomorphs, and $\overline{T}$ = the mean thickness obtained from a linear trace across the specimen surface. The use of this equation implicitly assumes the allotriomorphs to be plates, having uniform thickness and a random spatial distribution.

The specimens used for transmission electron microscopy were prepared from the 0.25 mm × 13 mm × 13 mm sheets by standard grinding and jet-polishing techniques. Jet-polishing was performed with either a chrome-acetic-acid electrolyte at 21 °C, or a 1 pct perchloric acid–methanol electrolyte at −68 °C. Ion beam milling was sometimes performed on the jet-polished specimens to expand the electron transparent areas.

Conventional transmission electron microscopy was performed on a Philips EM 301 operated at 100 kV. Convergent beam electron diffraction and energy dispersive X-ray spectroscopy (EDS) were performed on a Philips EM 400 operated at 100 kV. Because of an objectionably high Cu K_α systems background, EDS results will be reported only qualitatively.

III. RESULTS

The TTT diagrams generated for the Fe-1.43C and the Fe-1.49C-4.90Cu alloys are shown in Figure 2. The equilibrium austenite:(austenite + cementite) solvus temperature for the Fe-1.43C alloy was 970 °C.[26] The equilibrium austenite:(austenite + cementite + ε-Cu) solvus temperature for the Fe-1.49C-4.90Cu alloy was also approximately 970 °C.[25] The transformation start curves in these diagrams represent the first observation of product phases by optical metallography. The dotted portions of the curves indicate that transformation times less than six seconds were not practical with the experimental technique used.

Figure 2 shows that the initiation of the pearlite transformation was significantly delayed by copper. The effects of copper on the pearlite transformation are reported elsewhere.[29]

The proeutectoid cementite transformation start curves for the Fe-1.43C and the Fe-1.49C-4.90Cu alloys were found to be the same. Individual grain boundary allotriomorphs, such as those shown in Figure 3, were sometimes observed at the start of the proeutectoid cementite reaction. Because of the quickness of this precipitation, a severe quench from the transformation temperature was necessary to stop it at its early stages. However, the iced-brine quench that was used also induced cracking along the austenite grain boundaries, and this severely limited the number of unimpinged allotriomorphs that could be observed. Nevertheless, from the observations that were made, it was clear that for identical heat treatments, the allotriomorphs in both alloys had similar size and shape distributions. The average aspect ratio of these allotriomorphs tended to be about 5:1.

The morphology of the proeutectoid cementite at later stages of isothermal transformation was also substantially the same in the Fe-C and the Fe-C-Cu alloys. Figure 4 shows optical micrographs of the microstructures produced in Fe-1.43C and Fe-1.49C-4.90Cu, by transformation at 800 °C, for one minute. Proeutectoid cementite, in thin film morphology, covers nearly all of the austenite grain boundaries. The thicknesses of these grain boundary films were nearly the same for both alloys. The true thicknesses of the films in Fe-1.43C and Fe-1.49C-4.90Cu were 1.6 microns and 1.5 microns, respectively.

Figure 5 shows the microstructures produced in Fe-1.43C and Fe-1.49C-4.90Cu, by transformation at 750 °C, for one minute. The thicknesses of the grain boundary films of proeutectoid cementite were nearly the same in both alloys.

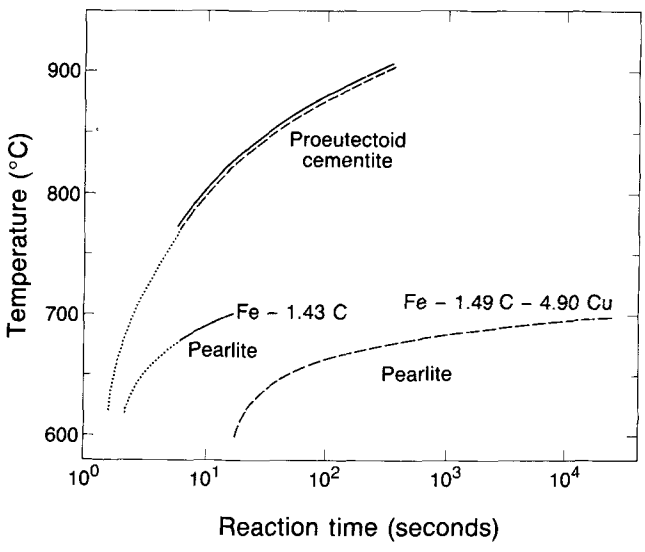

Fig. 2—TTT diagrams for Fe-1.43C and Fe-1.49C-4.90Cu.

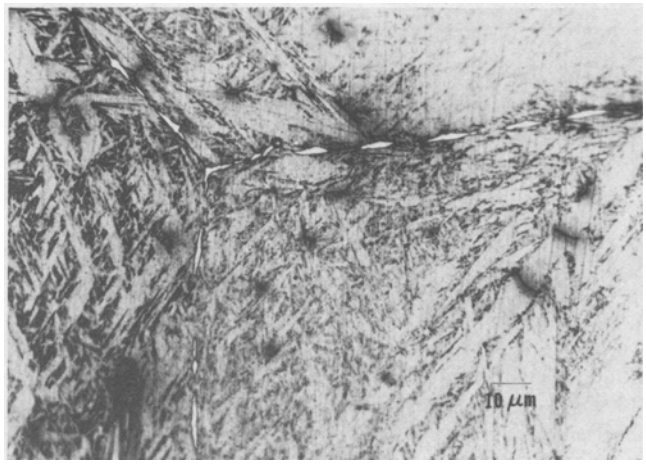

Fig. 3—Optical micrograph of proeutectoid cementite grain boundary allotriomorphs produced in Fe-1.49C-4.90Cu by transformation at 825 °C, for one min.

Both of these microstructures also contained many intragranular proeutectoid cementite Widmanstätten plates. The lengths of the longest plates were also nearly the same for both microstructures, about 115 microns.

Although optical microscopy revealed little influence of copper on the morphology of the proeutectoid cementite, the effect of copper on the fine structure of that phase was readily apparent by transmission electron microscopy. The proeutectoid cementite in the Fe-C-Cu alloys was found to contain fine precipitates. Figure 6 represents a typical transmission electron microscope observation of the proeutectoid cementite that was produced in Fe-1.49C-4.90Cu by transformation at 750 °C for one minute. The bright-field image, Figure 6(a), shows a high density of strongly diffracting particles within a cementite matrix. Energy dispersive X-ray microanalysis indicated that these precipitates were rich in copper. By electron diffraction, these precipitates have been identified as the face-centered-cubic ε-Cu phase. Because the ε-Cu precipitates were small and embedded in the cementite matrix, the reflections belonging to them generally had low intensity in the selected area diffraction patterns. They were usually identified by systematically displacing the objective aperture so that it surrounded each of the ε-Cu reflections, and then making double exposures.

The dark-field image of the ε-Cu precipitates, Figure 6(b), indicates that nearly all of them share a common $[\bar{1}1\bar{1}]\varepsilon$-Cu reciprocal lattice vector and that they are distributed throughout the cementite, right up to the cementite: austenite interphase boundary that existed just prior to the iced-brine quench. No ε-Cu precipitates were observed

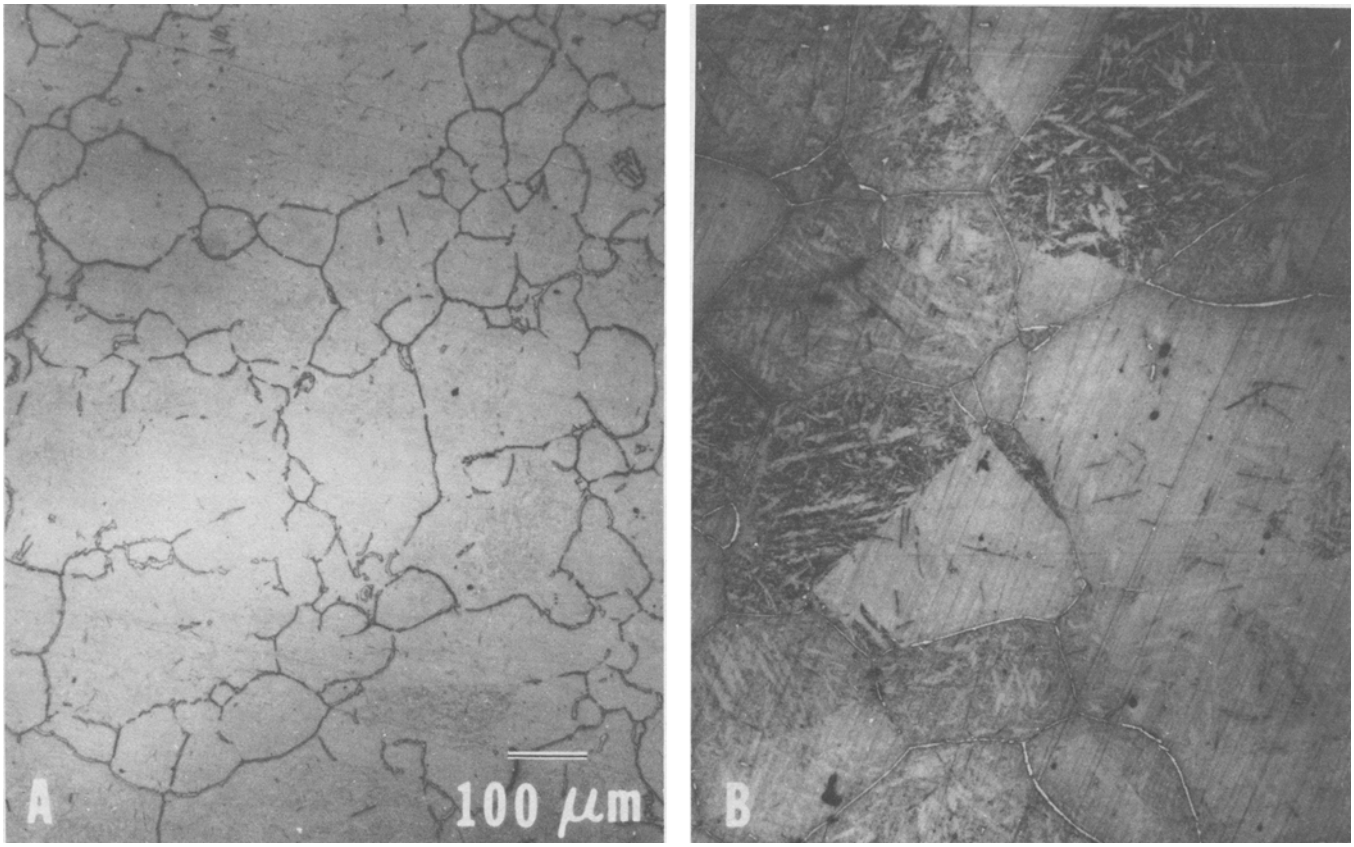

Fig. 4—Optical micrographs of proeutectoid cementite that was produced in Fe-1.43C (*a*) and Fe-1.49C-4.90Cu (*b*), by transformation at 800 °C, for one min.

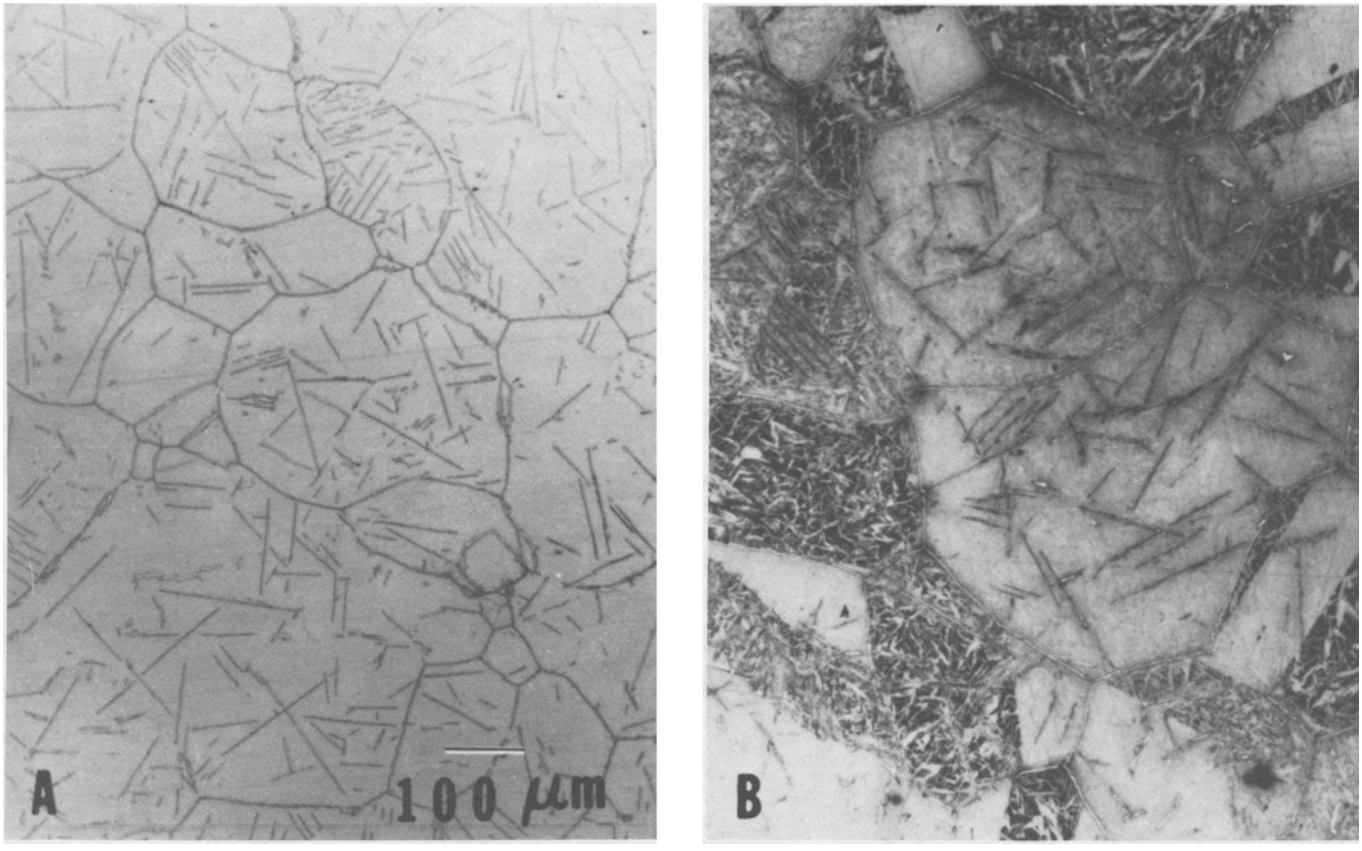

Fig. 5—Optical micrographs of proeutectoid cementite that was produced in Fe-1.43C (*a*) and Fe-1.49C-4.90Cu (*b*), by transformation at 750 °C, for one min.

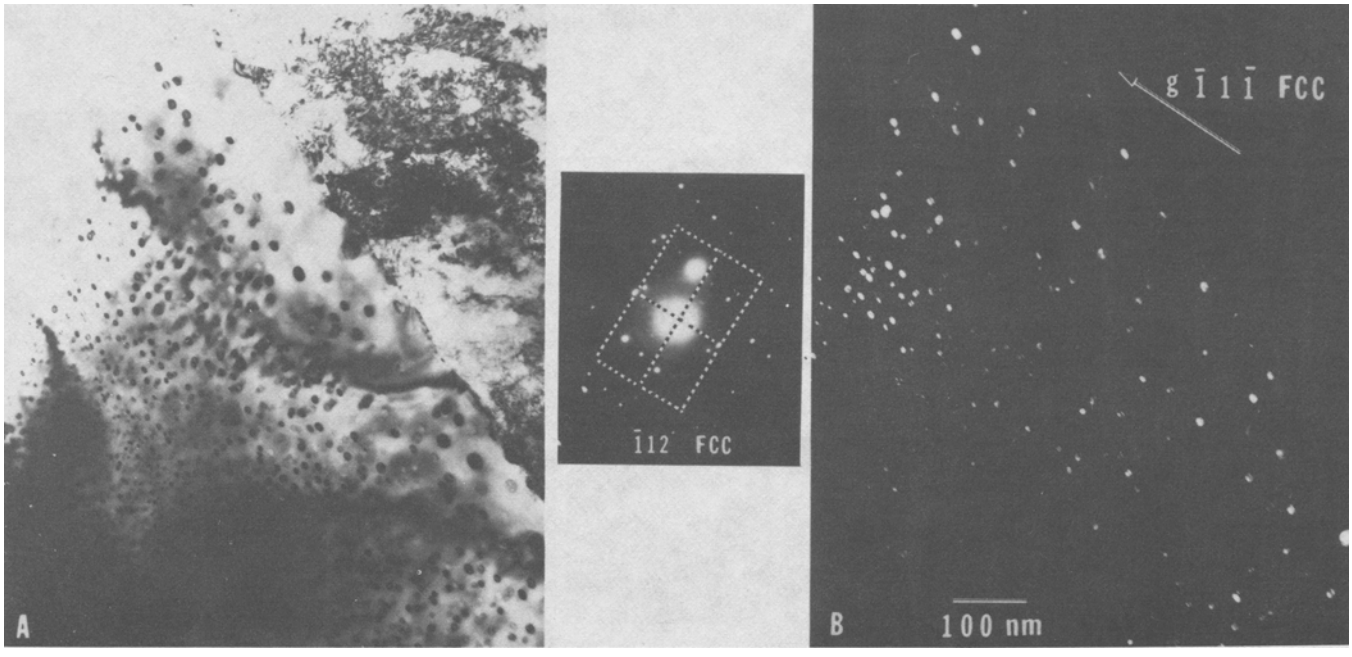

Fig. 6—(*a*) Bright-field transmission electron micrograph of proeutectoid cementite, face-centered-cubic ε-Cu, and martensite that was produced in Fe-1.49C-4.90Cu by transformation at 750 °C, for one min, followed by an iced-brine quench. The included selected area diffraction pattern shows that the beam direction was nearly parallel to the $[\bar{1}12]\varepsilon$-Cu zone axis. (*b*) Dark-field image taken with the $\mathbf{g}[\bar{1}1\bar{1}]\varepsilon$-Cu reflection.

within the adjacent martensite* (austenite before iced-brine quenching). No retained austenite was observed in these microstructures, which is surprising in view of their high carbon content.

*The matrix in these microstructures is a mixture of martensite and bainite. The one quality of this matrix that is critical to the current work is its crystallographic orientation relationship with the parent austenite. Since both martensite and bainite are usually related to austenite by relationships close to that of Kurdjumov-Sachs or Nishiyama-Wasserman,[30,31] the matrix will be loosely referred to as martensite.

In the bright-field micrograph, Figure 6(a), the ε-Cu particles decrease in size, from about 400 Å to about 150 Å, as the distance from the cementite:martensite interphase boundary increases. The micrograph also shows that the distance from the interphase boundary to the position where the ε-Cu precipitates are of minimum size is about 0.6 microns, which corresponds to the true half-thickness of the grain boundary cementite films shown in the optical micrograph of this microstructure, Figure 5(b).

It was consistently found that the ε-Cu precipitates within the proeutectoid cementite were crystallographically related to the martensite which abutted the cementite. The orientation relationship between these phases was generally found to be very close to that of Nishiyama-Wassermann. An example of this is illustrated in Figure 7, which shows the microstructure produced in Fe-1.31C-3.57Cu by isothermal transformation at 800 °C for 190 minutes. The convergent beam electron diffraction patterns show the parallelism of the [121]ε-Cu and [110]martensite zone axes, as well as the reciprocal lattice vectors $\mathbf{g}[\bar{1}1\bar{1}]\varepsilon$-Cu and $\mathbf{g}[\bar{1}10]$martensite. The dark-field micrograph, Figure 7(b), taken with the nearly coincident $\mathbf{g}[\bar{1}1\bar{1}]\varepsilon$-Cu and $\mathbf{g}[\bar{1}10]$ martensite reflections, indicates that nearly all of the ε-Cu precipitates are of the same crystallographic variant. No ε-Cu precipitates were found in the adjacent martensite. The Figure 7 micrographs again show that the ε-Cu precipitates decrease in size as the distance from the cementite:martensite interphase boundary increases. The arrows point to an ε-Cu precipitate that was in the process of forming at the cementite:austenite interphase boundary just prior to the iced brine quench. The higher transformation temperature and longer transformation time used to produce this microstructure gave a wider range of ε-Cu precipitate sizes than that shown in Figure 6.

The smallest ε-Cu precipitates in these microstructures took shapes that were approximately spherical or cuboidal. The largest precipitates, however, often took shapes that were more anisotropic. A large angle tilting experiment revealed that the three-dimensional shape of the largest ε-Cu particles tended to be that of thick platelets. This is illustrated in Figure 8, which shows ε-Cu precipitates within proeutectoid cementite that was produced in Fe-1.35C-3.5Cu by isothermal transformation at 800 °C for 190 minutes. In Figure 8(a) the electron beam direction is nearly parallel to [010]CEM.* The traces of (100)CEM and (001)CEM are indicated in the figure. The arrow points to an ε-Cu precipitate with a projected aspect ratio of 4.4:1. Figure 8(b) shows the same area after being tilted through an angle of 80 deg about $\mathbf{g}[001]$CEM. It can be seen that the projected aspect ratio of the ε-Cu precipitate has decreased in a manner that is consistent with its being a thick platelet, having dimensions of approximately 160 × 490 Å × 700 Å. The projected shapes of the other ε-Cu precipitates in Figure 8 can be seen to respond similarly to tilting. In this case the platelets lie on (100)CEM; however, other habit planes were also observed.

*Throughout this text the convention used to describe the dimensions of the cementite orthorhombic unit cell will be that which has been traditionally used by metallurgists, $a < b < c$.[32]

When the ε-Cu precipitates were small (<300 Å), their density was high, and their spatial distribution was

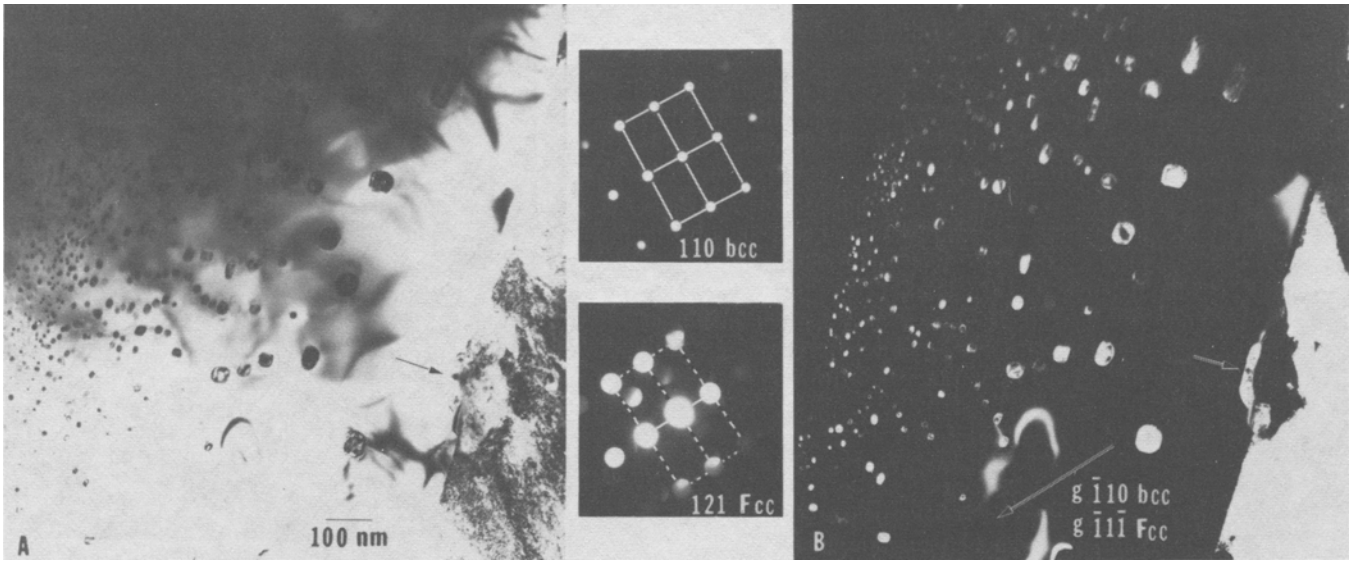

Fig. 7—(*a*) Bright-field transmission electron micrograph of proeutectoid cementite, face-centered-cubic ε-Cu. and martensite that was produced in Fe-1.31C-3.57Cu by transformation at 800 °C, for 190 min, followed by an iced-brine quench. (*b*) Dark-field image, taken with the nearly coincident $\mathbf{g}[\bar{1}1\bar{1}]\varepsilon$-Cu and $\mathbf{g}[\bar{1}10]$martensite reflections. The included convergent beam electron diffraction patterns shows that the ε-Cu and the martensite are Nishiyama-Wasserman related.

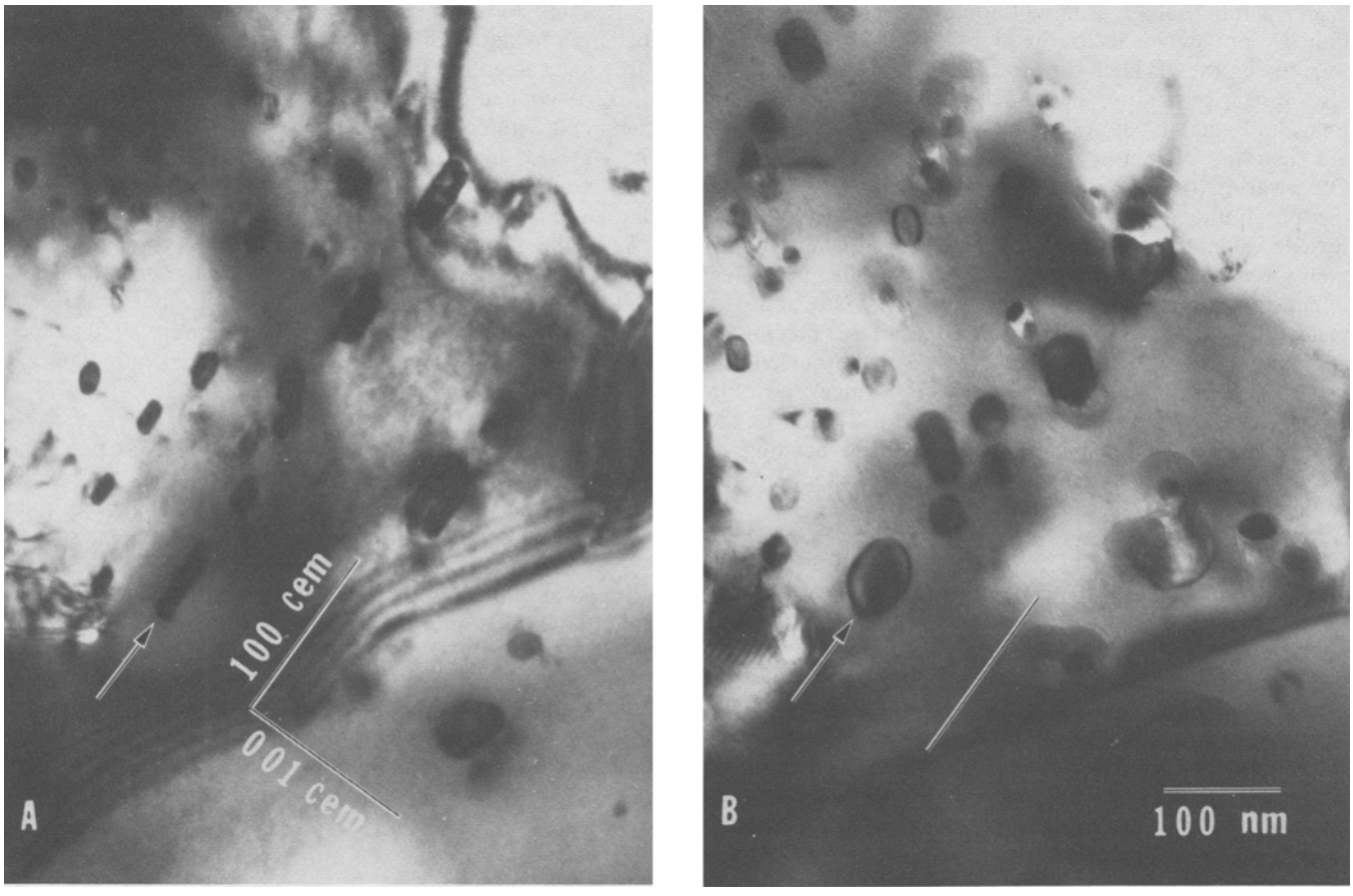

Fig. 8—Bright-field transmission electron micrographs of ε-Cu precipitates within proeutectoid cementite that was produced in Fe-1.31C-3.57Cu by transformation at 800 °C for 190 min. (*a*) The electron beam is nearly parallel to [010]CEM, and the traces of (100)CEM and (001)CEM are shown. (*b*) The same area after being tilted through an angle of 80 deg about **g**[001]CEM.

apparently random. Extensive tilting of the specimens and observation of stereo pairs failed to reveal any consistent and systematic distributions of these small precipitates.

Although the small ε-Cu precipitates always appeared to be randomly distributed, the larger precipitates, produced by long isothermal transformations, were often found to be systematically distributed. An example of this is shown in Figure 9, which shows ε-Cu precipitates within proeutectoid cementite that was produced by transformation at 800 °C for 190 minutes. There it can be seen that as the ε-Cu precipitates increase in size, from about 100 Å to about 500 Å, their spatial distribution changes from apparently random to apparently regularly-spaced linear arrays.

Nearly all of the ε-Cu precipitates shown in Figure 9 exhibit Moiré fringes. The selected area diffraction pattern, included in Figure 9, indicates that this micrograph was taken with two beam diffracting conditions very nearly satisfied for both the ε-Cu and the cementite. The incident beam direction is close to both [110]ε-Cu and [010]CEM. These Moiré fringes are a consequence of double diffraction between the nearly coincident **g**[103]CEM and **g**[$1\bar{1}1$]ε-Cu reflections. Some of the ε-Cu precipitates exhibit fringes that are almost exactly perpendicular to **g**[103]CEM, indicating that they are parallel Moiré fringes. Others, especially the smaller ones, are definitely of mixed character, *i.e.*, rotation and parallel.

The parallel Moiré fringe spacing, D, can be calculated from the following equation:[33,34] $D = d_1 d_2 / [d_1 - d_2] = M d_2$, where M is called the 'Moiré magnification'. Using the values $d_1 = d(111)\varepsilon\text{-Cu} = 2.087$ Å,[35] and $d_2 = d(103)\text{CEM} = 2.013$ Å,[32] the parallel Moiré fringe spacing was calculated to be 56.7 Å. The average parallel Moiré fringe spacing measured from Figure 9 was 53 Å, which agrees well with the calculated value. The angle of rotation of Moiré fringes, W, is related to the angle of rotation between the ε-Cu and cementite crystals, θ, by the Moiré magnification, $W = M\theta$. The largest measured rotation of the Moiré fringes in Figure 9 was 40 deg, which, with $M = 28.2$, gave a calculated value of $\theta = 1.4$ deg. Therefore, Figure 9 indicates that for this orientation, *i.e.*, nearly parallel [110]ε-Cu and [010]CEM zone axes, the ($1\bar{1}1$)ε-Cu and (103)CEM lattice planes match up very well, but that small angular displacements do exist.

Although the orientation relationship between ε-Cu and the martensite which abutted the cementite was consistently found to be close to Nishiyama-Wasserman, several different orientation relationships were observed between ε-Cu and cementite. The orientation relationship that was most frequently observed led to the Moiré fringes shown in Figure 9. It is illustrated in the selected area electron diffraction pattern shown in Figure 10. This diffraction pattern indicates that the [110]ε-Cu and [010]CEM zone axes are

nearly parallel, and that in addition to the previously mentioned near coincidence of the $\mathbf{g}[1\bar{1}1]\varepsilon$-Cu and $\mathbf{g}[103]$CEM reflections, the $\mathbf{g}[1\bar{1}\bar{1}]\varepsilon$-Cu and $\mathbf{g}[200]$CEM reflections are also in near proximity, about 7 deg apart. The bright-field image in Figure 10 shows some large ε-Cu precipitates that are near the cementite:martensite interphase boundary. Observation of the change in the projected shape of the precipitates after tilting far away from [010]CEM revealed that these precipitates were thick platelets with their broad faces parallel to (010)CEM. The projected dimensions of the largest ε-Cu precipitate are approximately 930 Å × 1700 Å. The long edges of this precipitate are close to being parallel to the trace of the cementite: martensite interphase boundary. The Moiré fringes shown in Figure 10 are not perfectly straight. The distortion of the fringes must have been caused by localized bending of the specimen.[34] Bend contours can also be seen in the cementite matrix.

IV. DISCUSSION

During the growth of proeutectoid cementite in the Fe-C-Cu alloys, copper was partitioned away from the cementite by the precipitation of ε-Cu. Both the kinetics and the microstructure of the transformation indicate that this precipitation of ε-Cu took place at the cementite:austenite interphase boundaries, and that interphase boundary diffusion of copper was an essential part of this process.

It is unlikely that any significant partitioning of copper occurred by lattice diffusion into the austenite, ahead of the growing cementite. This would have required a diffusive flux of copper into austenite which was already supersaturated with copper. The diffusivity of copper in austenite was also much too low to allow such a flux to exist. The extent to which copper could have been pushed into the austenite may be estimated by the ratio D_{Cu}/G, where D_{Cu} = the lattice diffusion coefficient of copper in austenite, and G = the thickening rate of the cementite.[36,37] Although the thickening of proeutectoid cementite grain boundary allotriomorphs diminishes rapidly at the later stages of the transformation,[6] the initial thickening appears to be approximately parabolic in time,[5] *i.e.*, $L = A(Dt)^{1/2}$, where L = the allotriomorph half-thickness, D = the diffusion coefficient for carbon in austenite, A = the parabolic rate constant, and t = the growth time. The effective value of $AD^{1/2}$ can be evaluated by inserting the appropriate experimental values of allotriomorph half-thickness and growth time.[37] For example, for Fe-1.49C-4.90Cu, transformed at 800 °C, the growth time was about 50 seconds, and the allotriomorph half-thickness was measured to be 7.5×10^{-5} cm. These values give $AD^{1/2} = 1.06 \times 10^{-5}$ cm/sec$^{1/2}$. The thickening rate can be determined by differentiation, giving $dL/dt = G = AD^{1/2}/2t^{1/2}$. Using the value of $AD^{1/2}$ just calculated, the growth rate, at $t = 50$ seconds, was $G = 7.5 \times 10^{-7}$ cm/sec. The diffusion coefficient for copper in austenite, at 800 °C, is

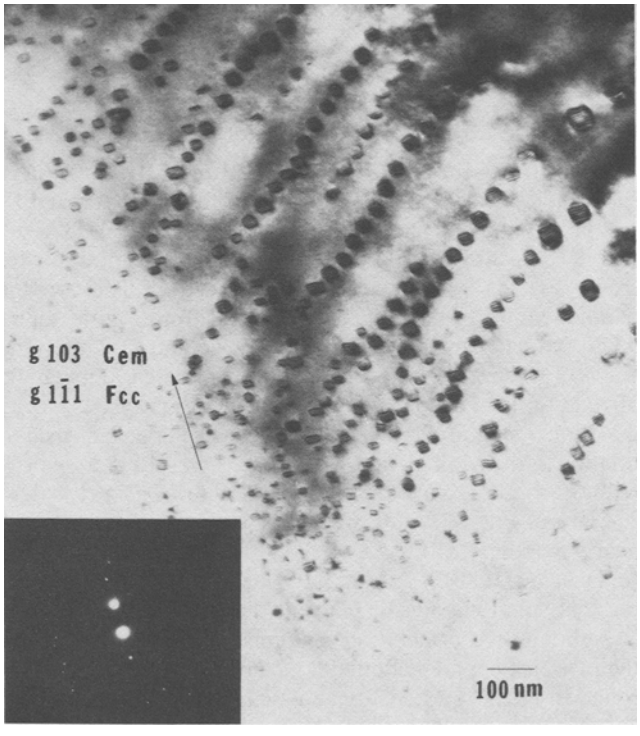

Fig. 9—Bright-field transmission electron micrographs of face-centered-cubic ε-Cu precipitates within proeutectoid cementite that was produced in Fe-1.31C-3.57Cu by transformation at 800 °C for 190 min. The included selected area diffraction pattern shows that the two-beam conditions of $\mathbf{g}[103]$CEM and $\mathbf{g}[1\bar{1}1]\varepsilon$-Cu were simultaneously satisfied.

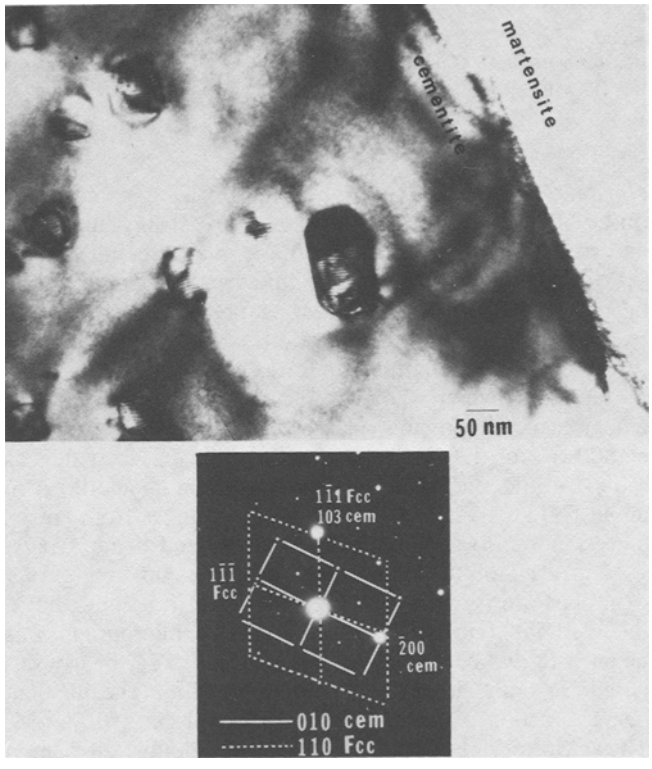

Fig. 10—Bright-field transmission electron micrograph showing ε-Cu precipitates within proeutectoid cementite that was produced in Fe-1.31C-3.57Cu by transformation at 800 °C for 190 min. The included selected area diffraction pattern shows that [010]CEM and [110]ε-Cu zone axes are nearly parallel. The nearly coincident $\mathbf{g}[103]$CEM and $\mathbf{g}[1\bar{1}1]\varepsilon$-Cu reflections are responsible for the Moiré fringes.

9.7×10^{-15} cm^2/sec.[38] Therefore the distance that copper could have been pushed into the austenite, by lattice diffusion, was limited to distances of approximately D_{Cu}/G = 1.3 Å. This extremely small diffusion distance indicates that the cementite was always growing into austenite that had a constant concentration of copper, and that a high diffusivity path, provided by the cementite austenite interphase boundary, was responsible for the observed rapid precipitation of ε-Cu. Preliminary *in situ* heating studies in a high voltage electron microscope confirm this explanation.[39]

There are also several microstructural features which indicate that the ε-Cu was precipitated at the cementite: austenite interphase boundaries. The observation that the size of the ε-Cu precipitates decreased as the distance from the cementite:martensite interphase boundary increased indicates that the last ε-Cu precipitates to form, during the isothermal transformation, grew to be the largest. If the ε-Cu precipitates grew by boundary diffusion, then their size should have been directly related to the length of time that they were in contact with the boundary. The observed size distribution therefore implies that the velocity of the interphase boundary decreased as the transformation progressed, which is consistent with the known thickening behavior.[5,6] The observation of an ε-Cu precipitate that was in the process of growing at the cementite:austenite interphase boundary, just prior to the iced-brine quench (arrowed precipitate in Figure 7), is another indicator of precipitation at interphase boundaries.

The observation that nearly all of the ε-Cu precipitates took the same variant of crystallographic orientation relationships with both the cementite and the adjacent martensite indicates that the cementite:austenite interphase boundary acted as a common heterogeneity for ε-Cu nucleation. The adoption of a single crystallographic variant is a trait that appears to be common to all types of interphase precipitates.[12-16] The variant taken is often the one that promotes the formation of low energy interfaces between both of the phases which form the boundary. The activation free energy for nucleation is thereby reduced.[12,13,19]

Since martensite and bainite are usually Kurdjumov-Sachs or Nishiyama-Wasserman related to austenite,[30,31] the consistently observed N-W orientation relationship between ε-Cu and martensite indicates that the ε-Cu was cube:cube related to the austenite. This is expected since the lattice parameters of high carbon austenite and ε-Cu are very similar;[35] hence the {111} planes of these fcc phases must have matched very well.

Although it appears that a cube:cube relationship was always maintained between ε-Cu and austenite, the ε-Cu established several different orientation relationships with the cementite. Presumably, all of these orientation relationships promoted the formation of low energy ε-Cu: cementite interfaces. Inspection of stereographic projections revealed that the orientation relationship which was most often encountered, $[010]CEM \| [110]\varepsilon\text{-Cu}$, $(103)CEM \| (1\bar{1}1)\varepsilon\text{-Cu}$, is also the same as that which has been observed between proeutectoid cementite Widmanstätten plates and retained austenite.[40] A reason for this orientation relationship can be found in the fact that the cementite crystal structure is such that the {103} planes possess the highest density of iron atoms,[32] and so the close-packed planes of the two phases tend to parallelism.

Despite the extensive partitioning of copper that was accomplished by interphase precipitation of ε-Cu, the great similarities in the thicknesses of the grain boundary allotriomorphs and the lengths of the Widmanstätten plates that were produced in identically transformed specimens of Fe-1.43C and Fe-1.49C-4.90Cu, indicate that the growth rates of proeutectoid cementite were substantially the same in both alloys. As has been found by previous researchers,[5,6] the thicknesses of the allotriomorphs indicate that these growth rates were less than those allowed by the diffusion of carbon through austenite. The half-thickness that the allotriomorphs would be expected to take, if their growth was diffusion controlled, may be estimated by the equation, $L = A(Dt)^{1/2}$.[2] For a planar growth front, the parabolic rate constant is approximately:[2,41]

$$A = \frac{(C^{\gamma} - C^{\gamma:c})}{[(C^{c} - C^{\gamma})(C^{c} - C^{\gamma:c})]^{1/2}}$$

where C^{γ} = the carbon concentration of the alloy, $C^{\gamma:c}$ = the carbon concentration of austenite in contact with the cementite, and C^{c} = the carbon concentration of the cementite. Taking $C^{\gamma:c}$ and C^{c} from the 800 °C tie-line of the Fe-C phase diagram, the parabolic rate constant for the Fe-1.43C alloy is 0.09. The diffusivity of carbon in austenite, at 800 °C, increases by almost a factor of three as the carbon concentration increases from $C^{\gamma:c}$ to C^{γ}.[42] Taking the weighted average as the effective diffusion coefficient,[43,44] $D = 9.0 \times 10^{-8}$ cm^2/sec. For a growth time of 50 seconds, $L \approx 1.9$ microns. For transformation at 800 °C, with a growth time of about 50 seconds, the Fe-1.43C alloy exhibited an allotriomorph half-thickness of 0.8 microns, which is about 40 pct of the theoretical value.

Thickening rates lower than those allowed by the diffusion of carbon through austenite are also exhibited by proeutectoid ferrite grain boundary allotriomorphs.[7] Although models based on the assumption that growth is controlled by carbon diffusion cannot account for the observed thickening rates, it has been demonstrated that they are of great use in explaining the relative differences in the allotriomorph thickening kinetics observed in Fe-C and ternary alloys. Within this context, an alloying element exerts its influence primarily by altering the concentration gradient of carbon.[45,46] When Fe-C and ternary alloys of similar carbon content are compared, the change in concentration gradient imparted by the alloying element can be obtained from the appropriate phase diagrams. In the absence of partitioning, the influence of the alloying element can be qualitatively described by the difference between the phase boundaries in the Fe-C equilibrium phase diagram and the "no-partition equilibrium", or "paraequilibrium" phase diagram of the ternary alloy.[36,45] However, the present data make it clear that despite the sizable (>200 °C) undercoolings from the equilibrium solvus temperatures, the conditions of paraequilibrium were not obtained in the Fe-C-Cu alloys—interphase precipitation of ε-Cu was always observed. Under these conditions, the austenite contacting the interphase boundary must have had a carbon concentration that was much closer to that of austenite in three phase (austenite + cementite + ε-Cu) equilibrium. The Fe-C-Cu phase diagram, Figure 1, shows that the carbon concentration of austenite, in three phase equilibrium, is nearly identical to

that of austenite in an Fe-C binary alloy. Since the Fe-1.43C and the Fe-1.49C-4.90Cu alloys had similar carbon contents, the carbon concentration gradient, and therefore the flux of carbon to the cementite, were probably not affected much by copper.

The similar allotriomorph thickening kinetics exhibited by Fe-1.43C and Fe-1.49C-4.90Cu also indicate that the ε-Cu precipitates did not act as a structural obstacle to allotriomorph growth. In the early stages of proeutectoid cementite precipitation, the allotriomorph growth rates were high, and the interphase boundaries were densely populated with ε-Cu precipitates. If these precipitates had interfered with growth, by pinning mobile interphase boundaries, then it is likely that the proeutectoid cementite growth kinetics in Fe-1.49C-4.90Cu would have been much lower than those in Fe-1.43C. The absence of any great decrease in growth kinetics implies that the precipitation of ε-Cu took place on the portions of the interphase boundary that were partially coherent, and therefore inherently immobile.[18] The similar thickening kinetics also indicate that the abundance of partially coherent facets was similar in both the Fe-1.43C and the Fe-1.49C-4.90Cu alloys.

Since the cementite:austenite interphase boundary was destroyed by the martensitic transformation that occurred during the iced-brine quench, a direct determination of the exact proportion of partially coherent interphase boundaries could not be ascertained by electron microscopy. However, the high density of ε-Cu precipitates that was produced at the early stages of the transformation indicates that when the cementite growth rates were high, the cementite:austenite interphase boundary contained a large number of partially coherent facets. The absence of any large systematic distributions of small ε-Cu precipitates also implies that when the cementite growth rates were high, the partially coherent facets did not extend over large distances, and that the growth ledges associated with the facets were also not very high. The observations of relatively smooth cementite:martensite interphase boundaries also indicate that ledge heights were not great. This is in contrast to the broad, planar sheet distributions of interphase precipitates that have been produced during ferrite growth in some hypereutectoid steels.[12,13] The transition from a dense, apparently random distribution of small ε-Cu precipitates to curved, linear arrays of larger precipitates reflects the increased boundary diffusion distances that were associated with decreased proeutectoid cementite growth rates.

V. CONCLUSIONS

The following conclusions have been reached concerning the effects of copper on the isothermal precipitation of proeutectoid cementite:

1. Copper does not have a large influence on the kinetics of proeutectoid cementite precipitation. In both Fe-C and Fe-C-Cu alloys, proeutectoid cementite grain boundary allotriomorphs thicken at rates that are considerably less than those allowed by the diffusion of carbon through austenite.
2. Copper can be partitioned during the growth of proeutectoid cementite by the precipitation of ε-Cu at cementite:austenite interphase boundaries. Both the microstructural and the kinetic data indicate that interphase boundary diffusion of copper was an essential part of this precipitation. Because the proeutectoid cementite grain boundary allotriomorphs in Fe-1.43C and Fe-1.49C-4.90Cu exhibited similar thickening kinetics, it was also concluded that these ε-Cu precipitates did not impede boundary migration by pinning mobile interphase boundaries.

ACKNOWLEDGMENTS

This work was supported by the Director, Office of Energy Research, Materials Sciences Division of the United States Department of Energy under Contract No. DE-AC03-76SF00098. Valuable discussions with Dr. Uhlrich Dahmen during the course of this work are gratefully acknowledged.

REFERENCES

1. R. W. Heckel and H. W. Paxton: *Trans. AIME*, 1970, vol. 53, p. 539.
2. H. I. Aaronson: *Decomposition of Austenite by Diffusional Processes*, Interscience, New York, NY, 1962, p. 387.
3. W. T. Reynolds, Jr., M. Enomoto, and H. I. Aaronson: *Phase Transformations in Ferrous Alloys*, TMS-AIME, Warrendale, PA, 1984, p. 115.
4. G. Krauss: *Metall. Trans. A*, 1978, vol. 9A, p. 1527.
5. R. W. Heckel and H. W. Paxton: *Trans. TMS-AIME*, 1960, vol. 218, pp. 799-806.
6. T. Ando and G. Krauss: *Acta Metall.*, 1981, vol. 29, pp. 351-63.
7. J. R. Bradley, J. M. Rigsbee, and H. I. Aaronson: *Metall. Trans. A*, 1977, vol. 8A, pp. 323-33.
8. W. S. Owen: *J. Iron Steel Inst.*, 1951, vol. 167, p. 117.
9. L. S. Darken: *Trans. TMS-AIME*, 1961, vol. 221, p. 654.
10. T. Ando and G. Krauss: *Metall. Trans. A*, 1981, vol. 12A, pp. 1283-90.
11. J. Fridburg and M. Hillert: *Acta Metall.*, 1970, vol. 18, pp. 1253-60.
12. R. W. K. Honeycombe: *Metall. Trans. A*, 1976, vol. 7A, pp. 317-21.
13. R. W. K. Honeycombe: *Phase Transformations in Ferrous Alloys*, TMS-AIME, Warrendale, PA, 1984, p. 259.
14. R. A. Ricks, P. R. Howell, and R. W. K. Honeycombe: *Metall. Trans. A*, 1979, vol. 10A, pp. 1049-58.
15. R. A. Ricks, P. R. Howell, and R. W. K. Honeycombe: *Met. Sci.*, 1980, vol. 14, pp. 562-68.
16. R. A. Ricks: *J. Matl. Sci.*, 1981, vol. 16, pp. 3006-12.
17. R. A. Ricks and P. R. Howell: *Acta Metall.*, 1983, vol. 31, pp. 853-61.
18. T. Obara, G. J. Shiflet, and H. I. Aaronson: *Metall. Trans. A*, 1983, vol. 14A, pp. 1159-67.
19. H. I. Aaronson, M. R. Plichta, G. W. Franti, and K. C. Russel: *Metall. Trans. A*, 1978, vol. 9A, pp. 363-71.
20. G. J. Shiflet, H. I. Aaronson, and J. R. Bradley: *Metall. Trans. A*, 1981, vol. 12A, pp. 1743-50.
21. A. Stosuy and M. Ohring: *Copper in Iron and Steel*, I. LeMay and L. McDonald Schetky, eds., J. Wiley & Sons, New York, NY, 1982.
22. L. Habraken and J. Lecomte-Beckers: *Copper in Iron and Steel*, I. LeMay and L. McDonald Schetky, eds., J. Wiley & Sons, New York, NY, 1982, p. 45.
23. M. C. Sneed, J. L. Maynard, and R. C. Brasted: *Comprehensive Inorganic Chemistry*, D. VanNorstrand Co., New York, NY, 1954, vol. II, p. 110.
24. A. Hultgren: Kungl. Svenska Vetenskapsakademiens Handlingar, 1953, vol. 4, No. 3, pp. 1-47.
25. B. Uhrenius: *Hardenability Concepts with Applications to Steels*, D. V. Doane and J. S. Kirkaldy, eds., ASM, Warrendale, PA, 1976.
26. M. Hansen: *Constitution of Binary Alloys*, 2nd ed., McGraw-Hill, New York, NY, 1958, p. 353.
27. J. R. Bradley and H. I. Aaronson: *Metall. Trans. A*, 1977, vol. 8A, pp. 317-22.

28. R. L. Fullman: *Trans. AIME*, 1953, vol. 197, pp. 447-52.
29. J. A. Wasynczuk: Ph.D. Thesis, University of California, Berkeley, CA, 1985.
30. B. V. Narashima Rao and G. Thomas: *Proc. ICOMAT 1979*, MIT Press, Cambridge, MA, 1979, pp. 12-21.
31. J. W. Christian and D. V. Edmonds: *Phase Transformations in Ferrous Alloys*, TMS-AIME, Warrendale, PA, 1984, p. 293.
32. H. Lipson and N. J. Petch: *J. Iron Steel Inst.*, 1940, vol. 142, p. 95.
33. G. Thomas and M. J. Goringe: *Transmission Electron Microscopy of Materials*, J. Wiley and Sons, New York, NY, 1979, p. 90.
34. P. B. Hirsch, A. Howie, R. B. Nicholson, D. W. Pashley, and M. J. Whelan: *Electron Microscopy of Thin Crystals*, 2nd ed., R. E. Krieger Co., Malabar, FL, 1977, p. 353.
35. W. B. Pearsons: *Lattice Spacings and Structures of Metals and Alloys*, Pergamon Press, New York, NY, 1958, p. 570, p. 919.
36. M. Hillert: *Solid-Solid Phase Transformations*, TMS-AIME, Warrendale, PA, 1982, p. 789.
37. K. R. Kinsman and H. I. Aaronson: *Metall. Trans.*, 1973, vol. 4, pp. 959-67.
38. G. R. Speich, J. A. Gula, and R. M. Fisher: *The Electron Microprobe*, J. Wiley and Sons, New York, NY, 1966, p. 525.
39. G. Thomas: *In Situ Experiments with High Voltage Electron Microscopes*, Proc. of Int. Symp. on HVEM, Osaka, Japan, Nov. 18-20, 1985, p. 351.
40. W. Pitsch: *Acta Metall.*, 1962, vol. 10, pp. 897-99.
41. C. Zener: *J. Appl. Phys.*, 1949, vol. 20, pp. 950-53.
42. C. Wells, W. Batz, and R. F. Mehl: *Trans. AIME*, 1950, vol. 188, pp. 553-60.
43. L. Kaufman, S. V. Radcliff, and M. Cohen: *Decomposition of Austenite by Diffusional Processes*, Interscience, New York, NY, 1962, p. 313.
44. R. Trivedi and G. M. Pound: *J. Appl. Phys.*, 1967, vol. 38, p. 3569.
45. H. I. Aaronson, H. A. Domian, and G. M. Pound: *Trans. TMS-AIME*, 1966, vol. 236, pp. 768-81.
46. J. R. Bradley and H. I. Aaronson: *Metall. Trans. A*, 1981, vol. 12A, pp. 1729-41.